Macromolecules
ARTICLE
pubs.acs.org/Macromolecules

Enhanced Performance in Lithium–Polymer Batteries Using Surface-Functionalized Si Nanoparticle Anodes and Self-Assembled Block Copolymer Electrolytes

Ilyoung Choi,[†] Hyungmin Ahn,[‡] and Moon Jeong Park*,[†,‡]

[†]Division of Advanced Materials Science (WCU) and [‡]Department of Chemistry, Pohang University of Science and Technology (POSTECH), Pohang, Korea 790-784

ABSTRACT: We have explored new Li–polymer batteries composed of surface functionalized Si nanoparticles (SiNPs) as anode active materials and nanostructured block copolymers as solid electrolytes. Surface protection of SiNPs with poly(ethylene oxide) chains successfully prevents aggregation of SiNPs during cycling and also helps fast Li^+ transport to the active centers in the anodes. The self-assembly nature of block copolymer electrolytes in ca. 50 nm periodicity is aimed to restrain the formation of macroscopic ionic clusters during Li-insertion/desertion. To decouple the electrical and mechanical properties of polymer electrolytes, two different nonvolatile additives (ionic liquid and non ionic plasticizer) were incorporated and remarkably different cycle performances have been observed. The incorporation of ionic liquid yields the utmost ionic conductivity and distinctly large first lithium insertion capacity of 2380 mA h/g was seen. However, the formation of solid electrolyte interphase (SEI) was responsible for highly irreversible lithium desertion capacity and the system indicate fast capacity fading during cycling. With the use of non ionic plasticizer, in contrast, the SiNPs anode can store lithium up to a reversible capacity of ~1850 mA h/g under aggressive test profiles of 80 °C and voltage window between 0–4.5 V. The focused ion beam technique was successfully used to obtain ex-situ transmission electron microscopy images of cycled polymer electrolytes and anode materials to underpin the origin of capacity retention or fading upon cycling. The results suggest that the structural retention of both polymer electrolytes and SiNPs during cycling attributes to the improved battery performance.

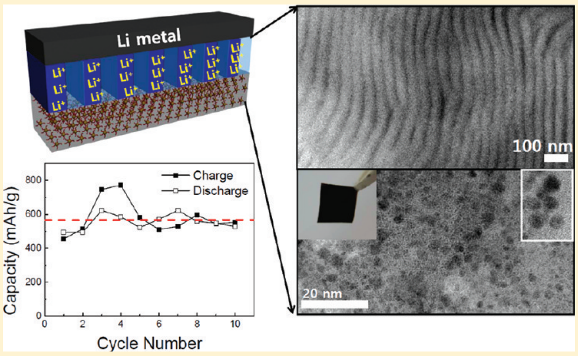

INTRODUCTION

In recent years Li-batteries have attracted significant interests for a variety of applications such as portable electronics and electric vehicle (EV) batteries due to their high energy densities.[1,2] Although, Li-batteries have already been widely used in portable electronics, the development of a commercial Li-battery powered EV that replaces a gasoline powered vehicle, aimed to relieve global warming, is still painstakingly slow. Key challenges in advancing the technology lie in specific energy density (>200 W h kg^{-1}), the long-term cycle properties (1,000 charge/discharge cycles), and durability at elevated temperature (operating temperature −40 to 85 °C).[3]

Significant efforts have been devoted to replace commercial graphite anode (theoretical capacity of 370 mA h g^{-1}) by a wide range of anode active materials such as Si,[4] Ge,[5] and Sn[6] elements due to their high theoretical capacity of 4200, 1600, and 990 mA h g^{-1}, respectively. However, their practical usage in Li-ion batteries appears to be distant since the long-term cycle property is hampered by huge volume changes of above elements during Li-insertion/desertion cycles.[7] The volume changes eventually result in the loss of electrical contact between the active material and the current collector.[8] One of appealing solutions to solve these issues is the use of nanometer-sized anode active materials[4−6,8−15] such as nanoparticles (NPs)[5a,10−12] and nanowires (NWs)[4,5b,13,14] so that the anodes can accommodate large strain originated from volume changes during cycling.

With regard to the durability issues, the replacement of the liquid electrolytes with solid polymer electrolytes is essential on account of (1) the potential risk of fire and (2) decomposition reactions of liquid electrolytes at high cell potential. Polymer electrolytes composed of salts and polymers can offer ionic conductivity in solid form and poly(ethylene oxide) (PEO) based polymer electrolytes have been extensively studied to date.[16−18] However, the lack of mechanical stability of PEO chains owing to the low glass transition temperature (T_g) limits the battery cycle properties.[18] To decouple conductivity and mechanical properties, a variety of polymer electrolyte systems have been proposed; example includes (1) dry polymer electrolytes containing stiff polymer chains,[19−22] (2) composite polymer electrolytes,[23−25] and (3) polymer gel electrolytes.[26] Despite numerous reports on conductivities of the different polymer electrolytes, relatively limited numbers of studies are concerning cycle performances of

Received: April 5, 2011
Revised: July 13, 2011
Published: August 25, 2011

dx.doi.org/10.1021/ma200796k | *Macromolecules* 2011, 44, 7327–7334

Li−polymer batteries by varying conductivity, morphology, and mechanical property of polymer electrolytes.[22,23,26c,26d,27]

Herein, we were motivated to prepare high performance Li-polymer battery by optimizing the electrical and mechanical properties of both anode materials and polymer electrolytes. First, as anode active materials, the system of interest consists of uniformly sized SiNPs, functionalized with Li^+ conducting PEO chains. PEO chains at the surface of SiNPs act as protective layers, preventing aggregation of SiNPs during cycling. Furthermore, the PEO chains help fast Li^+ transport to the active centers in the anodes. This is in sharp contrast to the methodologies of carbon coating[28] or surface capping with short alkyl chains[29] on the nanoobjects surfaces. In fact, even the particles were well covered by carbon layers or short alkyl chains, the anode active materials were easily pulverized during the early stages of cycling.[28,29]

As solid electrolytes, in present study, we have used a PEO-based block copolymer, poly(styrene-*b*-ethylene oxide) (PS−PEO, 40.5-*b*-30.8 kg/mol), blended with PEO (3.4 kg/mol) homopolymer. In these systems, the conducting pathways are provided by PEO chains while a nonconducting PS block imparts the mechanical stability at high temperature up to 100 °C.[19] In particular, self-assembly nature of the PS−PEO copolymer in nanometer scales attributes to the restrained formation of macroscopic ionic clusters during Li insertion/desertion. To develop methodologies for decoupling the electrical and mechanical properties of polymer electrolytes, three major strategies are identified: (1) use of dry PS−PEO/PEO electrolyte; (2) incorporation of PS-selective, nonionic additive (dimethyl phthalate, DMP, $T_b = 283$ °C) into the PS−PEO/PEO mixture; (3) impregnation of PEO-selective, nonvolatile ionic liquid (1-ethyl-3-methylimidazolium tetrafluoroborate, $[EMIm][BF_4]$) into the PS−PEO/PEO mixture. We have investigated the proposed Li−polymer battery under aggressive test profiles of 80 °C and voltage window between 0 and 4.5 V to alleviate the durability concerns at elevated temperature.

■ EXPERIMENTAL SECTION

Synthesis of PEO−SiNPs. Inside a glovebox, $SiCl_4$ (100 μL) and tetraoctylammonium bromide (1.5 g) were dissolved in toluene (100 mL), and the solution was stirred for 1 h. Lithium aluminum hydride in THF (1 M, 2 mL) was added slowly, followed by stirring for 3 h. The H-terminated SiNPs (H-SiNPs) were collected by the addition of methanol (20 mL). Hydrosilylation of H-SiNPs was then performed by adding ω-allyl-terminated PEO methyl ether (MW = 1310 g mol^{-1}, 0.5 g, Polymer Source) and $HPtCl_6 \cdot 6H_2O$ (0.1 M, 100 μL) catalyst. The mixture was stirred for 3 h. The resulting PEO−SiNPs were extracted into water with sonication, and unreacted reagents were further removed by dialysis (cellulose acetate bag, Spectrum Laboratories, MWCO 2 kDa).

Synthesis of Polymer Electrolytes. The poly(styrene-*b*-ethylene oxide) (PS−PEO, 40.5-*b*-30.8 kg mol^{-1}, M_w/M_n = 1.08) is synthesized by sequential high-vacuum anionic polymerization as described in ref 30. The PEO homopolymer (M_w = 3.4 kg mol^{-1}) was purchased from Sigma-Aldrich. PEO chains are doped with $LiClO_4$ salts where the ratio of $[Li^+]/[EO]$ was fixed as 0.056. 10 wt % solutions of PS−PEO/PEO mixture containing 1-ethyl-3-methylimidazolium tetrafluoroborate (HPLC grade, Sigma-Aldrich) or dimethyl phthalate (≥99%, Sigma-Aldrich) were prepared using 50/50 vol % THF and methanol mixture. Solutions were stirred overnight at room temperature, and the dried samples were pressed into 300 μm thick disks using a mechanical press with pressures of up to 2000 psi at 80 °C. The through-plane conductivity of different polymer electrolytes was measured using a homemade test cell on thermostated pressed samples, using a Solartron 1260 frequency response analyzer connected to a Solartron 1296 dielectric interface. All procedures were performed inside the glovebox with oxygen and moisture level of 0.1 ppm.

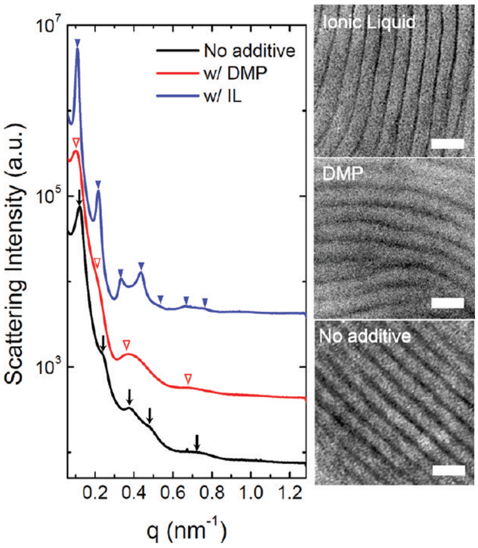

Figure 1. SAXS profiles and TEM images of PS−PEO/PEO electrolytes in the presence or absence of additives. The loading level of DMP and ionic liquid is 30 and 10 wt %, respectively. The scattering profiles are vertically offset for clarity. The arrows (↓, neat), the inverted open triangles (▽, DMP), and the inverted filled triangles (▼, ionic liquid) indicate Bragg peaks at q^*, $2q^*$, $3q^*$, $4q^*$, $6q^*$; at q^*, $2q^*$, $3q^*$,$4q^*$; and at q^*, $2q^*$, $3q^*$, $4q^*$, $5q^*$, $6q^*$, $7q^*$; respectively. TEM images of no additive, DMP, and ionic liquid incorporated PS−PEO/PEO copolymers represent qualitatively similar lamellar morphology. The salt-doped PEO domains were darkened by RuO_4 staining, and the scale bars represent 100 nm.

Preparation of Coin-Type Half-Cells. The composite anode materials for the battery testing were prepared by mixing PEO−SiNPs, super P carbon black, and poly(vinylidene fluoride) (PVDF, Solef) in a weight ratio of 8:1:1 with aid of *N*-methyl-2-pyrrolidone (NMP, Aldrich). The coin-type half-cell consists of the composite anode materials, polymer electrolytes, and Li foil. No separator was used. The loading of active material was 2 mg/cm^2, and the same charge and discharge rates of 0.1 mA were used for entire cycling tests.

Ex-Situ FIB−TEM Experiments of Cycled Anodes. For the ex-situ TEM analysis of the cycled samples, cross-sectional anode materials and polymer electrolytes were prepared with a FEI Strata 235 dual beam FIB using 30 keV Ga^+ beam and a Leica Ultracut UCT (−120 °C), respectively. Samples were characterized with a JEOL JEM-2100F microscope operated at 200 kV. X-ray diffraction analysis on anode materials was carried out at 8C2 beamline (λ = 1.5418 Å) of Pohang Accelerator Light Source (PAL) equipped with a MAR345 imaging plate detector. Synchrotron SAXS measurements on the polymer electrolytes before/after cyclings were performed using the 4C1 SAXS beamline at the PAL.

■ RESULTS AND DISCUSSION

Figure 1 describes the morphologies of three polymer electrolyte systems by combining small-angle X-ray scattering (SAXS) and transmission electron microscopy (TEM) experiments. For the dry PS−PEO/PEO electrolyte, the PS−PEO and PEO are blended with a weight ratio of 1:1 where the PEO phase is doped with $LiClO_4$ salts at a fixed concentration of $[Li^+]/[EO] = 0.056$. The PS−PEO/PEO, is referred to as “no additive” sample, and the amount of incorporated ionic liquid and DMP is 10 and 30 wt %, respectively. The “no additive” sample exhibits lamellar

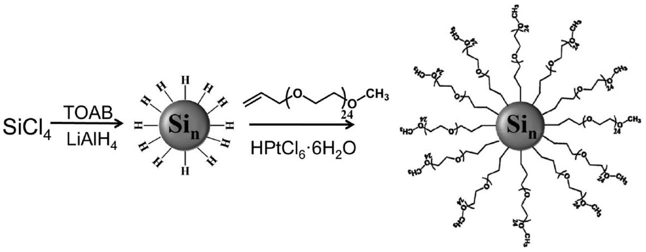

Figure 2. Synthesis of PEO-capped SiNPs.

morphology with Bragg peaks (↓) at $1q^*$, $2q^*$, $3q^*$, $4q^*$, and $6q^*$ where $q^* = 2\pi/d_{100}$ with d_{100} = 51.5 nm. Qualitatively similar SAXS peaks are observed with DMP added PS−PEO/PEO mixture, as shown by inverted open triangles (▽), where the presence of Bragg peaks at $1q^*$, $2q^*$, $3q^*$, and $6q^*$ with $q^* = 2\pi/d_{100}$ and d_{100} = 59.8 nm is seen. Note that 16% increase in domain size is seen upon adding 30 wt % DMP due to the swelling of PS domains. Although the SAXS profile indicative of lamellar structure is observed, it is evident that the degree of ordering in the sample becomes poor as seen from smeared high-order peaks. In contrast, when PEO-selective ionic liquid is incorporated to PS−PEO/PEO mixture, distinctly well-defined lamellar morphology is detected with Bragg peaks (▼) at $1q^*$, $2q^*$, $3q^*$, $4q^*$, $5q^*$, $6q^*$, and $7q^*$ where $q^* = 2\pi/d_{100}$ with d_{100} = 57.1 nm. This is presumably due to the increase in segregation strength between hydrophobic PS blocks and hydrophilic PEO blocks upon adding ionic moieties.

SAXS profiles in Figure 1 are confirmed by TEM experiments as shown in the inset TEM images (salt-doped PEO phases are darken by RuO$_4$ staining). Although all three polymer electrolytes show similar lamellar morphologies, it is evident that the lamellar structure of ionic liquid doped sample indicates sharp interface between hydrophobic and hydrophilic domains. This leads us to conclude that while the addition of either DMP or ionic liquid into lamellar forming PS−PEO/PEO mixture does not alter its morphology, the degree of ordering is affected. Note that the effects of degree of ordering on ionic conductivity for microphase-separated block copolymers are yet debating.[31,32] For example, Balsara et al. reported no significant changes in ionic conductivity for several PS−PEO block copolymer electrolytes upon undergoing order−disorder transition[31a] while Mahanthappa et al. and our group observed significantly enhanced conductivity with good long-range ordered polymer electrolytes.[31b,32] In following section, we will briefly discuss the data regarding the effect of long-range order on conductivity and cycle performance of our PS−PEO/PEO systems.

As anode active materials, the system of interest consists of uniformly sized SiNPs functionalized with PEO capping layers, aimed to prevent aggregation of SiNPs during Li insertion/desertion cycles. It is worthwhile to mention here that the use of PEO capping layers should help fast Li$^+$ transport into/out of SiNPs during charging/discharging cycles.[33] In addition, the PEO−SiNPs anode offers small interfacial resistance of battery cell by virtue of improved wetting between PEG-capped SiNPs and PEO blocks of PS−PEO/PEO electrolytes. Figure 2 shows the synthesis of PEO-capped SiNPs, hereafter, PEO−SiNPs, by reduction of silicon tetrachloride (SiCl$_4$) in the presence of lithium aluminum hydride (LiAlH$_4$) and tetraoctylammonium bromide (TOAB),[29] followed by hydrosilylation of H-SiNPs using alkene-functionalized PEO with aid of chloroplatinic acid (HPtCl$_6$·6H$_2$O) catalyst.[34] PEO−SiNPs are in white powder form, which is well soluble in both benzene and methanol, indicative of successful surface capping of SiNPs with PEO chains.

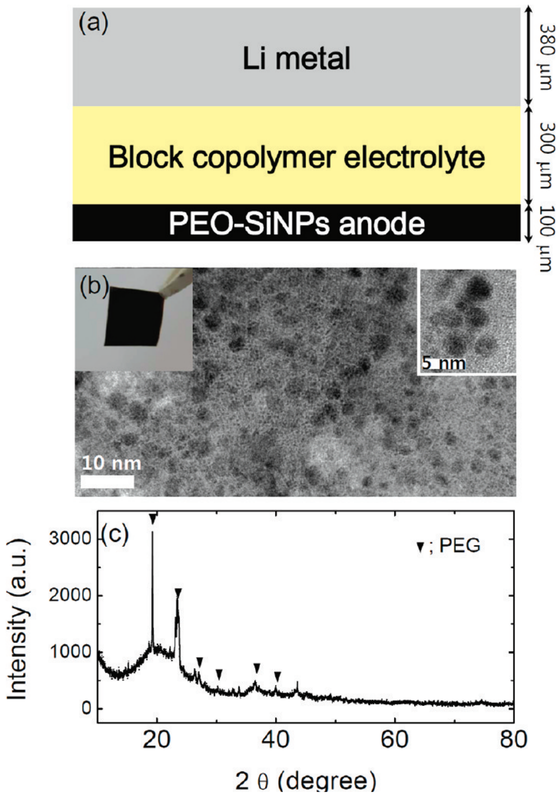

Figure 3. (a) A schematic illustration showing the coin-type half cell consists of Li metal, polymer electrolyte, and PEO−SiNPs composite anode. (b) FIB−TEM image of PEO−SiNPs composite anode. Photograph of the anode with 2 × 2 cm × 100 μm dimension is shown in the figure as an inset box. (c) XRD pattern of composite anode before cycling indicative of amorphous Si phase.

The chemical composition of PEO−SiNPs is measured by combining elemental analysis and thermogravimetric analysis, which yield the Si/EO stoichiometry of PEO−SiNPs as weight ratio between SiNPs and PEO capping layer as 4:6 (data not shown here). Since the average size of SiNPs used in present study is ca. 4 nm, each SiNP contains ∼1800 Si atoms,[35] and thus, the estimated number of PEO chains at the particle surfaces is 58. Accordingly, grafting density of PEO chains on the surface of SiNPs is 1.1/nm^2. To estimate the length of PEO capping layers, Flory radius (R_F) was calculated using the equation[36]

$$R_F = l_0\sqrt{MC_\infty/m_0} \tag{1}$$

where l_0 is the average backbone bond length of the polymer, M is molecular weight, C_∞ is the characteristic ratio, and m_0 is the monomer molecular mass per backbone. We used l_0 = 0.145 nm, C_∞ = 5.59, and m_0 = 14.7 from the literature[36] and the chain length ($2R_F$) of PEO capping layers with M_w = 1.3 kg/mol is estimated at 6.4 nm. Note that the PEO monomer size is 0.35 nm,[37] and the length of the fully stretched PEO chain ($L = l_0M/m_0$) is 12.9 nm. This implies that the size of PEO capping layers is large enough to keep the particle−particle distance against particle aggregation during the Li insertion/desertion.

The composite anodes are fabricated by integrating PEO−SiNPs, carbon (C), and poly(vinylidene fluoride) (PVDF) binders at a weight ratio of 8:1:1. PEO−SiNPs serves as an active

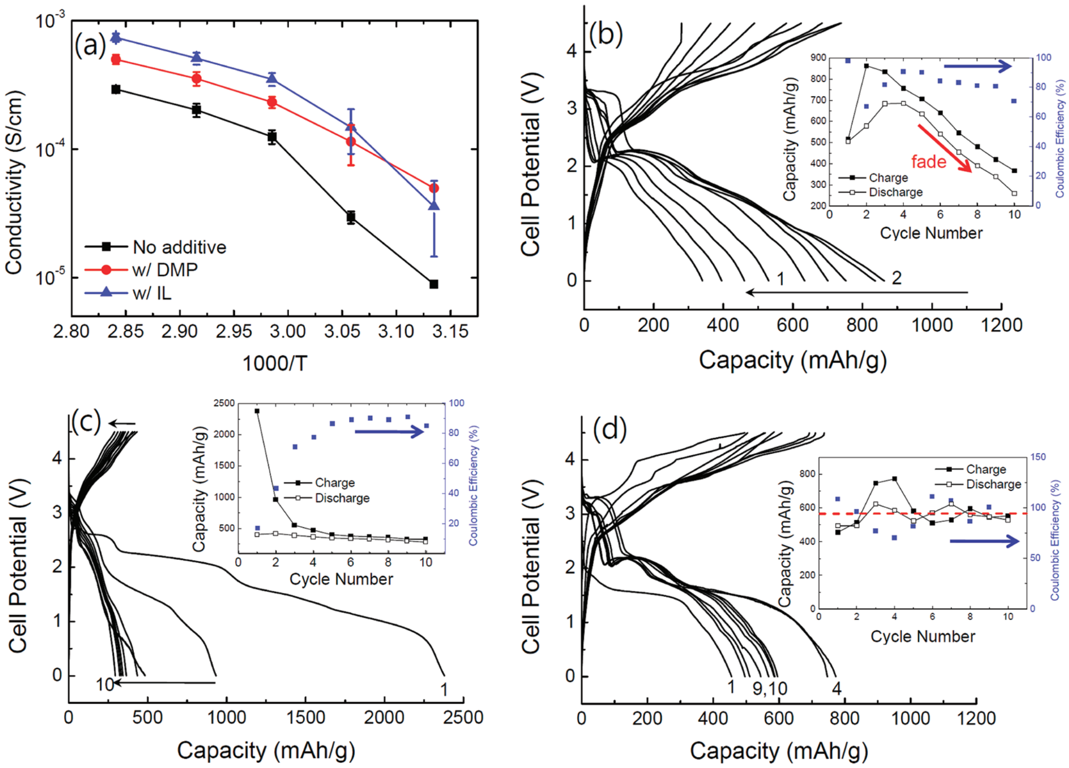

Figure 4. (a) Temperature-dependent ionic conductivities of PS−PEO/PEO electrolytes in the presence or absence of additives measured under anhydrous conditions. Galvanostatic charge/discharge curves of the PEO−SiNPs anode at the 0.1 mA between 0 and 4.5 V in coin-type half-cells using (b) PS−PEO/PEO electrolyte (no additive), (c) ionic liquid incorporated PS−PEO/PEO electrolyte, and (d) DMP-doped PS−PEO/PEO electrolyte. Charge/discharge capacities and Coulombic efficiency vs cycle number are plotted in right side of each voltage profile.

material, and C/PVDF are regarded as a supporting medium for electrical conductivity. In the literature,[38,39] it was reported that the PEO and PVDF are well miscible and improved ionic conductivity by 2 orders of magnitude is seen by introducing PVDF into PEO/salt systems. Accordingly, in our system, the PEO capping layers may help the adhesion of PEO−SiNPs to the conductive supporting medium layer, which leads to maintain large contact area.

Figure 3a shows representative graphics of a coin-type half-cell composed of Li-metal, block copolymer electrolyte, and PEO−SiNPs composite anode for battery testing. The typical thickness of Li metal, block copolymer electrolyte, and PEO−SiNPs anode is at around 380, 300, and 100 μm, respectively. Bright field cross-sectional TEM images of PEO−SiNPs composite anodes are given in Figure 3b. As can be seen from Figure 3b, the SiNPs with the average size distribution of 3.9 ± 0.6 nm are well-dispersed within the C/PVDF medium since the PEO capping layers prevent the aggregation of SiNPs. Note that the PEO layers are invisible in Figure 3b due to the lower electron contrast than Si atoms. The inset TEM image in Figure 3b obtained at higher magnification ensures the spherical shape of synthesized SiNPs. It should be also noted that the cross-sectional TEM samples of entire composite anodes examined in present study (before and after cycles) are prepared by a dual beam focused ion beam (FIB) instruments.[40] The conventional solution extraction method is excluded since the solvent-sensitive nature of lithiated anode active materials. The FIB−TEM experiments enable site-specific cross-sectioning of samples without perturbing the arrays of anode components, which are considered as more accurate analysis of SiNPs after electrochemical testing. The FIB−TEM experiments were performed in the presence of Cu current collector so that the heat damage during milling process is minimized by efficient heat transfer from anode materials to Cu substrate.

It is noteworthy that a large area, highly flexible free-standing PEO−SiNPs composite anode is readily fabricated by the solvent casting method. The dimension of anode typically employed in present study is 2 cm × 2 cm × 100 μm as shown in the inserted photograph of Figure 3b. It is also worthwhile to mention here that the synthesized SiNPs are amorphous as confirmed by both TEM (Figure 3b) and X-ray powder diffraction (Figure 3c). Formation of crystalline SiNPs requires higher temperatures due to the covalent nature of Si atoms, and at low-temperature amorphous phases become more common.[41] The inverted filled triangles (▼) in Figure 3c indicate well-known diffraction peaks from PEO chains.

We first examine the ionic conductivity of different polymer electrolytes under inert atmosphere conditions. In Figure 4a, the conductivity (σ) values of polymer electrolytes in the presence or absence of additives are plotted as a function of temperature from 45 to 80 °C, at a fixed $LiClO_4$ salt concentration of $[Li^+]/[EO] = 0.056$. As can be seen from the figure, with the increase in temperature the conductivity value increases owing to the enhanced charge transport. The temperature dependence of the ion conductivity in polymer electrolytes scales with the temperature dependence of the segmental motions, and thus the slope change at around 60 °C is due to the crystallinity of PEO chains (melting temperature of PEO is 55 °C). The addition of both nonionic plasticizer (DMP) and ionic liquid ($[EMIm][BF_4]$) results in enhanced conductivity where the maximum conductivity is obtained with the incorporation of ionic liquid. The origin of the increments in the conductivity of PS-selective DMP-doped samples is apparently due to the lowering T_g of PS chains while that in ionic liquid incorporated one is attributed to the amplified number density of ionic species in the sample. The obtained conductivity values are well located within the window of 10^{-4}–10^{-3} S cm^{-1} in the temperature range of 60–80 °C.

The galvanostatic charge/discharge voltage profiles of the PEO–SiNPs composite anode with three different polymer electrolyte systems described above were investigated between 0 and 4.5 V at a 0.1 mA (the charge and discharge rates were identical). The capacity values of each system up to 10 cycles are shown in Figure 4b–d. As shown in Figure 4b, for the case of "no additive" sample, the first charge (Li insertion process) and discharge (Li desertion process) capacities of 516 and 505 mA h g^{-1}, respectively, are observed. At the second cycle, both charge and discharge capacities increase to 863 and 579 mA h g^{-1}; however, gradual capacity fade was seen after 2 cycles, and the capacity retention after 10 cycles was only 39%. The Coulombic efficiency for the first cycle was 98%; however, the value decreases to 70% after 10 cycles.

When the ionic liquid doped polymer electrolyte is employed, which indicates the utmost ionic conductivity value, remarkably large charge capacity of 2380 mA h g^{-1} is seen in the first cycle, as shown in Figure 4c. This is 3 times higher than no additive case. However, the system shows highly irreversible charge/discharge behavior, i.e., low Coulombic efficiency of 18% for the first cycle, which is closely related to the intensive side reactions between the active materials and ionic species.[42] As a result, the charge capacity of the system is fast reduced to 934 mA h g^{-1} in the second cycle and eventually goes down below 300 mA h g^{-1} in the tenth charge cycle. The formation of the solid–electrolyte interface (SEI) layers is responsible for the large first charge capacity of the ionic liquid doped sample since Li^+ is further stored via charge separation of incorporated ionic moieties.[9,12,15] The gradual increase in Coulombic efficiency with the increase in cycle number implies the gradual decomposition of SEI layers upon cycling.[43]

Upon examining the battery performance composed of PEO–SiNPs composite anode and DMP doped polymer electrolyte, we observed notably different cycle behavior. As shown in Figure 4d, the system demonstrates first charge and discharge capacities of 456 and 495 mA h g^{-1}, respectively, corresponding to 109% Coulombic efficiency. These initial capacity values are smaller than other two systems. However, the charge capacity of the sample increases to 773 mA h g^{-1} in following cycle and then reaches to nice stable values of 555 (charge) and 565 mA h g^{-1} (discharge) upon increasing cycle number. As depicted in the inset plot of Figure 4d, in the initial 4 cycles, the Coulombic efficiency is fade from 109% to 76%; however, the values rise and converge to the values at 98 ± 9% from the sixth cycle. This result suggests that part of the Li_xSi is possibly left in the anode in the initial few cycles, and during the extended cycles, the residual Li_xSi can now access the polymer electrolyte to react back to Li^+ and Si during discharge cycles. We note in passing that when the same experimental protocols are repeated with commercial Si powder (average particle size is ca. 50 nm) using DMP-doped electrolyte, the voltage profiles indicate rapid capacity fade after only two cycles at 200 mA h g^{-1} (data not shown here) similar to the values in the literature.[44] It is evident that the optimization of not only anode active materials but also electrolytes is necessary to achieve the enhanced battery properties.

To underpin the cycle performance, TEM, XRD, and SAXS experiments have been performed on both block copolymer electrolytes and anode materials after cycling. As shown in Figure 5, it has been revealed that the morphologies of polymer electrolytes after cycling are sensitive function of the type of incorporated additives. The cross-sectional TEM micrographs of DMP incorporated electrolyte and ionic liquid doped sample, obtained after 10 cycles, are compared in Figures 5a and 5b, respectively. For the case on DMP incorporated sample, the TEM image in Figure 5a indicates well-ordered lamellar morphology with negligible change in domain spacing after 10 cycles. In contrast, as seen from Figure 5b, the TEM image of ionic liquid doped sample represents loss of long-range ordered microstructure and significantly enlarged domain sizes.

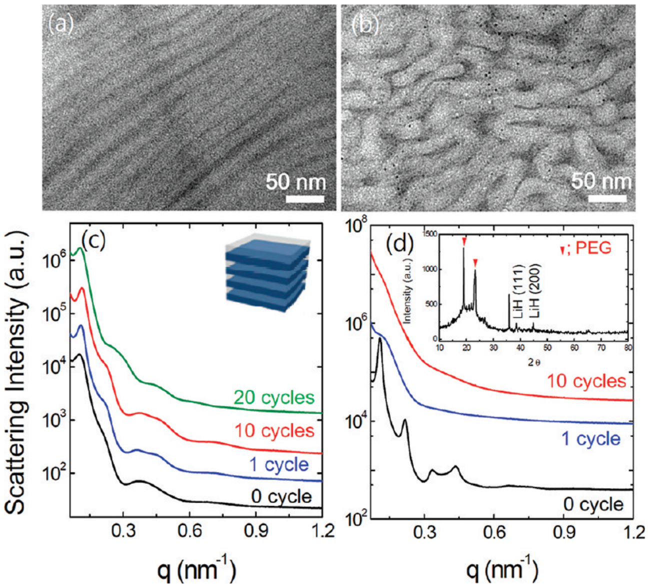

Figure 5. (a, b) Cross-sectional TEM images of polymer electrolytes after 10 cycles: (a) DMP-doped PS–PEO/PEO and (b) ionic liquid incorporated PS–PEO/PEO. The salt-doped PEO domains were darkened by RuO_4 staining. (c, d) SAXS profiles of PS–PEO/PEO electrolytes in the presence (c) DMP and (d) ionic liquid as a function of cycle number. The scattering profiles are vertically offset for clarity and cycle numbers are indicated in the figure. The inset figure in (d) shows XRD profile of ionic liquid doped PS–PEO/PEO mixture obtained after 10 charge/discharge cycles.

The TEM images in Figures 5a and 5b are confirmed by SAXS experiments and shown in Figures 5c and 5d. The ordered lamellae morphology of DMP incorporated sample is well-maintained even after 20 cycles with negligible changes in domain size and high order reflections. In contrast, the well-defined lamellar structure of ionic liquid doped sample was abruptly disrupted even after 1 cycle undoubtedly due to the formation of ionic clusters within the microstructure, which block the Li^+ transfer in the succeeding charging process. It is interesting to note here that the ionic liquid doped PS–PEO/PEO mixture is transparent at 80 °C before battery cycling; however, the sample becomes white and nontransparent after the cycle. The inset figure in Figure 5d shows XRD profile of ionic liquid doped PS–PEO/PEO mixture obtained after 10 charge/discharge cycles. The diffraction peaks at 38.4° and 44.9° indicate the formation of LiH crystallites within the polymer electrolyte.[45] The sharp diffraction peak at 35.9° is not clearly understood yet.

FIB–TEM and XRD experiments have performed on anode materials after cycling. As shown in Figure 6a, after 10 cycles, the

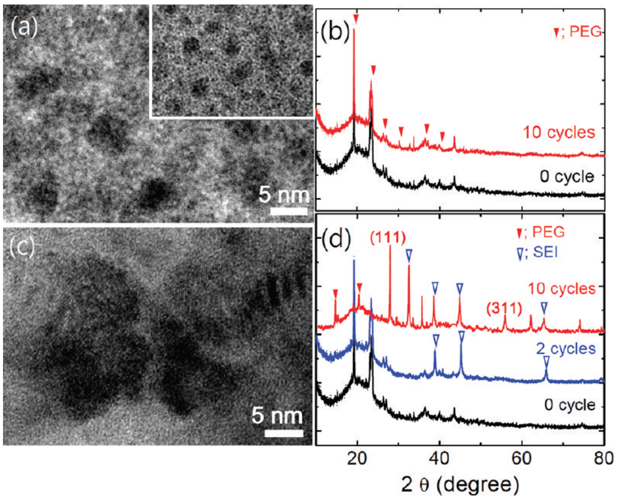

Figure 6. FIB−TEM images and XRD patterns of PEO−SiNPs anodes after 10 cycles; (a, b) PEO−SiNPs anode cycled with DMP-doped PS−PEO/PEO and (c, d) PEO−SiNPs anode cycled with ionic liquid incorporated PS−PEO/PEO. In (d) (111) and (311) indicate diffraction peaks from Si crystals.

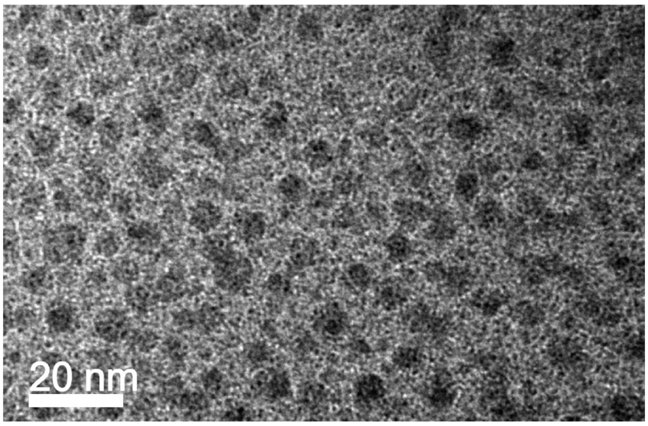

Figure 7. FIB−TEM image of PEO−SiNPs anode obtained after full lithium insertion cycle.

homogeneously distributed spherical SiNPs with smooth surface and average size of 3−5 nm have been observed. This is qualitatively similar feature obtained before cycling (Figure 3b). The inset TEM image in Figure 6a obtained with lower magnification indicates regularly spaced PEO−SiNPs after 10 cycles. The XRD pattern in Figure 6b also clearly indicates that the amorphous PEO−SiNPs appear to retain its pristine characteristics after cycling. The fact that the same SiNPs were seen after 10 cycles clearly demonstrates the role of PEO capping layers in maintaining the particle size and shape against aggregation and pulverization during cycling.

On the contrary, the anode materials cycled using ionic liquid doped polymer electrolyte reveal obviously different characteristics where largely aggregated particles with irregular surfaces are seen as shown in TEM image in Figure 6c. The XRD pattern in Figure 6d clearly indicates the formation of a variety of SEI phases after cycling; Li_2O (111) at 32.5°, LiH (111) at 38.5°, LiH (200) at 44.8°, and LiH (220) at 64.8°.[45] The unassigned peak at 35.9°, which was also seen from the cycled polymer electrolytes (Figure 5d), is consistently observed. It is interesting to mention here that after 10 cycles we began to observe diffraction peaks from Si crystal, which coexist with the SEI phases. At the same time the diffraction patterns originated from PEO capping layers are significantly distorted. This implies that particle aggregation and growth occur during Li insertion/desertion process, which attribute to the abrupt fade in cycle properties upon impeding the electrons and Li^+ transport, although we do not rule out the possibility of loss of electrical connection between the Si aggregates.

It is worthwhile to note here that when the fully charged anode materials are examined (no discharge cycle is followed), significant increases in particle sizes in range of 5−7 nm but still regularly spaced NPs are detected, as shown in Figure 7. This implies that the volume expansion upon inserting Li^+ is ca. 300−400% in our system, leading us to conclude that Li^+ can access most parts of the Si atom in the PEO−SiNPs. As reported in the literature,[46−48] during the Li insertion/desertion, stresses and strains are built up in the silicon anodes due to the large volume change. It can be assumed that SiNPs start to break up when the fracture stress reaches the Griffith−Irwin relation:[48]

$$\sigma_{\text{fracture}} = K/\sqrt{d} \tag{2}$$

where K is a constant related to the fracture toughness of the particles and d is particle size. Therefore, the improved stability in SiNPs during battery cycling is expected with the decrease in particle size.

Then, what would be the failure mechanism of "no additive" case? We carefully examined both block copolymer electrolyte and PEO−SiNPs composite anode following the same experimental methodologies described above. Figure 8a shows SAXS profiles of PS−PEO/PEO electrolyte in the absence of additives as a function of the cycle number. It is revealed that the ordered lamellae morphology of the "no additive" sample is gradually disrupted upon increasing the cycle number. Unlike DMP incorporated sample, the increases in the domain size as well as the low-q scattering intensity are also detected. In contrast, we observed the same amorphous characteristics of SiNPs after cycling with negligible detection of SEI layers, as shown in Figure 8b. In addition, as indicated by inverted filled triangles in the XRD pattern, the diffraction peaks from PEO appear to be unchanged.

Consequently, the possible origins of enhanced performances of Li−polymer battery composed of DMP-doped polymer electrolytes and PEO−SiNPs anodes are summarized as follows: (1) The DMP lowers T_g of PS phase offering enhanced ionic conductivity as well as the existence of soft additives can reduce ohmic resistance of the battery. (2) The PEG capping layers of SiNPs restrain particle aggregation during Li insertion/desertion, and the small particle size (ca. 4 nm) can reduce the elastic strain during battery cycling.

We hope to conclude our paper with addressing the importance of anode thickness to achieve high performance of Li battery. Figure 9 shows the charge and discharge curves when the battery capacity reaches to stabilized values. The battery cycling of the cells composed of 60, 30, and 20 μm thick anode has been performed at the same current value of 0.1 mA. As seen in the figure, the charge and discharge capacities of 60 μm thick anode were found to be 705 and 707 mA h g^{-1}, which are ∼30% increments in capacities compared to the values of 100 μm thick anode (Figure 4d). When the thickness of anode is further decreased to 30 μm, interestingly, we observed almost 2 times increase in charge and discharge capacities as 1390 and 1403 mA h g^{-1}. Even

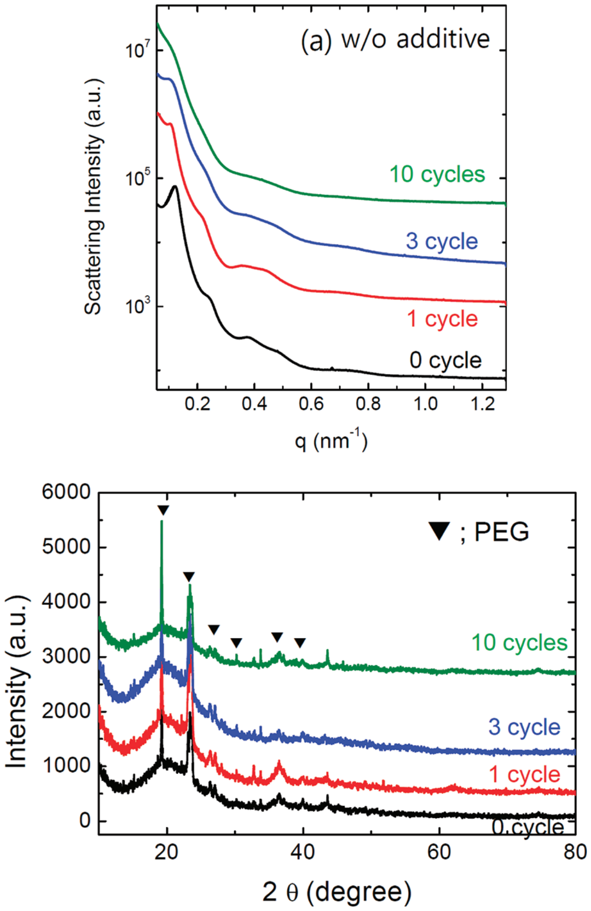

Figure 8. (a) SAXS profiles of PS—PEO/PEO electrolytes in the absence of additives as a function of cycle number. (b) XRD patterns of PEO—SiNPs anode cycled with "no additive" polymer electrolyte. The SAXS and XRD profiles are vertically offset for clarity and cycle numbers are indicated in the figure.

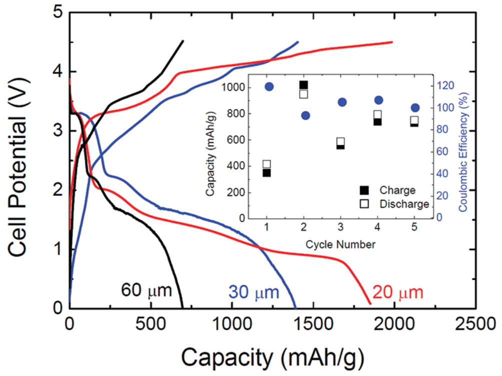

Figure 9. Charge/discharge voltage profiles of PEO—SiNPs composite anode between 0—4.5 V in coin-type lithium cells using DMP doped PS—PEO/PEO solid electrolyte where the capacity is sensitive function of anode thickness. The thicknesses of anode are indicated in the figure. Galvanostatic charge/discharge capacities and Coulombic efficiency of 60 μm thick PEO—SiNPs composite anode vs cycle number are shown in the inset figure.

further reduction in the anode thickness results in more enhanced charge and discharge capacities of 1851 and 1983 mA h g^{-1}, respectively. It is obvious that the optimization of anode thickness and kinds of polymer electrolytes can open possibility to obtain highly performing Li—polymer battery with capacity close to the theoretical values. We note in passing that regardless of the anode thickness, only for the batteries consisting of DMP doped polymer electrolytes, high Coulombic efficiency close to 100% is obtained once the battery becomes stabilized. In the inset figure of Figure 9, we plotted charge/discharge capacities and Coulombic efficiency of 60 μm thick PEO—SiNPs composite anode as a function of cycle number. It is also noted here that we were not able to make even thinner anode than 20 μm by solution casting due to the roughness and homogeneity issues, and future studies are needed to examine how the performance of PEO—SiNPs anodes changes with thicknesses down to submicrometers.

■ CONCLUSIONS

We have demonstrated a new strategy to produce high-performance Li—polymer battery by optimizing both polymer electrolytes and anode active materials. The enhanced cycling performance of Li—polymer batteries based on PEO—SiNPs as anode active materials benefits from restrained particle aggregation, elastic strain minimization, and fast Li$^+$ transport to the active centers. Self-assembled block copolymer electrolyte is an interesting model system to study the morphology effects on the performance of Li—polymer batteries with a flexible design in material compositions. It has been revealed that the addition of ionic liquid and/or hydrophobic plasticizer in block copolymer electrolytes results in enhanced ionic conductivity, which has been considered to be an important parameter in battery efficiency. However, the FIB—TEM results suggest that the structural retention of both block copolymer electrolytes during cycling is more critical issues to achieve the improved battery properties. For example, although the addition of ionic liquid into the block copolymer electrolyte indicates the utmost ionic conductivity value, the system shows highly irreversible charge/discharge behavior due to the intensive side reactions between the active materials and ionic species. In present study, upon utilizing surface functionalized SiNPs anode and nonionic hydrophobic plasticizer (DMP) incorporated block copolymer electrolyte, a reversible capacity of 1850 mA h g^{-1} is achieved under aggressive test profiles of 80 °C and voltage window between 0 and 4.5 V. Our work established a new methodology for improving the performance of Li—polymer batteries and thus impacts a broad spectrum of electrochemical systems. A fundamental study on the thickness effects of both anodes and block copolymer electrolytes will be the subject of future studies.

■ AUTHOR INFORMATION

Corresponding Author

*E-mail: moonpark@postech.edu.

■ ACKNOWLEDGMENT

This work was financially supported by Basic Science Research Program through the National Research Foundation of Korea (NRF) funded by the Ministry of Education, Science and Technology (Project No. 2011-0004375) and WCU (World Class University) program through the Korea Science and Engineering Foundation funded by the Ministry of Education, Science and Technology (Project No. R31-10059). SAXS and XRD measurements were conducted on the beamline 4C1 and 8C2 at the Pohang Light Source (PLS) supported by the Ministry of Science and

Technology of Korea. TEM and FIB experiments were performed at the National Nanofab Center supported by Korea Nano Technology Research Society (Project No. N100810002).

■ REFERENCES

(1) (a) Li, Y.; Tan, B.; Wu, Y. *Nano Lett.* **2008**, *8* (1), 265–270. (b) Park, J. C.; Kim, J.; Kwon, H.; Song, H. *Adv. Mater.* **2009**, *21*, 803–807.

(2) *Advances in Lithium-Ion Batteries*; van Schalkwijk, W., Scrosati, B., Eds.; Kluwer Academic/Plenum: Boston, 2004.

(3) Agrawal, R. C.; Pandey, G. P. *J. Phys. D: Appl. Phys.* **2008**, *41*, 223001–223018.

(4) (a) Chan, C. K.; Peng, H.; Liu, G.; McIlwrath, K.; Zhang, X. F.; Huggins, R. A.; Cui, Y. *Nature Nanotechnol.* **2008**, *3*, 31–35. (b) Park, M. H.; Kim, M. G.; Joo, J.; Kim, K.; Kim, J.; Ahn, S.; Cui, Y.; Cho, J. *Nano Lett.* **2009**, *9* (11), 3844–3847. (c) Cui, L. F.; Yang, Y.; Hsu, C. M.; Cui, Y. *Nano Lett.* **2009**, *9* (9), 3370–3374.

(5) (a) Lee, H.; Kim, H.; Doo, S. G.; Cho, J. *J. Electrochem. Soc.* **2007**, *154* (4), A343–A346. (b) Chan, C. K.; Zhang, X. F.; Cui, Y. *Nano Lett.* **2008**, *8* (1), 307–309.

(6) (a) Derrien, G.; Hassoun, J.; Panero, S.; Scrosati, B. *Adv. Mater.* **2007**, *19*, 2336–2340. (b) Meduri, P.; Pendyala, C.; Kumar, V.; Sumanasekera, G. U.; Sunkara, M. K. *Nano lett.* **2009**, *9* (2), 612–616.

(7) (a) Tarascon, J. M.; Armand, M. *Nature* **2001**, *414*, 359–367. (b) Meethong, N.; Huang, H. Y. S.; Speakman, S. A.; Carter, W. C.; Chiang, Y. M. *Adv. Funct. Mater.* **2007**, *17*, 1115–1123.

(8) (a) Hu, Y. S.; Guo, Y. G.; Sigle, W.; Hore, S.; Balaya, P.; Maier, J. *Nature Mater.* **2006**, *5*, 713–717. (b) Long, J. W.; Dunn, B.; Rolison, D. R.; White, H. S. *Chem. Rev.* **2004**, *104*, 4463–4492.

(9) Bruce, P. G.; Scrosati, B.; Tarascon, J. M. *Angew. Chem., Int. Ed.* **2008**, *47*, 2930–2946.

(10) Ma, H.; Cheng, F.; Chen, J.; Zhao, J.; Li, C.; Tao, Z.; Liang, J. *Adv. Mater.* **2007**, *19*, 4067–4070.

(11) (a) Graetz, J.; Ahn, C. C.; Yazami, R.; Fultz, B. *Solid-State Lett.* **2003**, *6*, A194–A197. (b) Kim, H.; Seo, M.; Park, M. H.; Cho, J. *Angew. Chem., Int. Ed.* **2010**, *49*, 2146–2149.

(12) Kim, M. G.; Cho, J. *Adv. Funct. Mater.* **2009**, *19*, 1497–1514.

(13) (a) Shaju, K. M.; Jiao, F.; Debart, A.; Bruce, P. G. *Phys. Chem. Chem. Phys.* **2007**, *9* (15), 1837–1842. (b) Park, M. S.; Wang, G. X.; Kang, Y. M.; Wexler, D.; Dou, S. X.; Liu, H. K. *Angew. Chem., Int. Ed.* **2007**, *46*, 750–753. (c) Armstrong, G.; Armstrong, A. R.; Bruce, P. G.; Reale, P.; Scrosati, B. *Adv. Mater.* **2006**, *18*, 2597–2600.

(14) Lee, Y. J.; Yi, H.; Kim, W. J.; Kang, K.; Yun, D. S.; Strano, M. S.; Ceder, G.; Belcher, A. M. *Science* **2009**, *324*, 1051–1055.

(15) (a) Guo, Y. G.; Hu, J. S.; Wan, L. J. *Adv. Mater.* **2008**, *20*, 2878–2887. (b) Wang, Y.; Cao, G. Z. *Adv. Mater.* **2008**, *20*, 2251–2269. (c) Lou, X. W.; Li, C. M.; Archer, L. A. *Adv. Mater.* **2009**, *21*, 2536–2539.

(16) (a) Fenton, D. E.; Parker, J. M.; Wright, P. V. *Polymer* **1973**, *14*, 589. (b) Armand, M. *Solid State Ionics* **1994**, *69*, 309–319.

(17) (a) Cho, B. K.; Jain, A.; Gruner, S. M.; Wiesner, U. *Science* **2004**, *305*, 1598–1601. (b) Wang, C. X.; Sakai, T.; Watanabe, O.; Hirahara, K.; Nakanishi, T. *J. Electrochem. Soc.* **2003**, *150*, A1166–A1170. (c) Kishimoto, K.; Yoshio, M.; Mukai, T.; Yoshizawa, M.; Ohno, H.; Kato, T. *J. Am. Chem. Soc.* **2003**, *125*, 3196–3197.

(18) Zhang, C.; Gamble, S.; Ainsworth, D.; Slawin, A. M. Z.; Andreev, Y. G.; Bruce, P. G. *Nature Mater.* **2009**, *8*, 580–584.

(19) (a) Singh, M.; Odusanya, O.; Wilmes, G. M.; Eitouni, H. B.; Gomez, E. D.; Patel, A. J.; Chen, V. L.; Park, M. J.; Fragouli, P.; Iatrou, H.; Hadjichristidis, N.; Cookson, D.; Balsara, N. P. *Macromolecules* **2007**, *40* (13), 4578–4585. (b) Panday, A.; Mullin, S.; Gomez, E. D.; Wanakule, N.; Chen, V. L.; Hexemer, A.; Pople, J.; Balsara, N. P. *Macromolecules* **2009**, *42* (13), 4632–4637.

(20) (a) Çelik, S. Ü.; Bozkurt, A. *Solid State Ionics* **2010**, *181*, 987–993. (b) Simone, P. M.; Lodge, T. P. *ACS Appl. Mater. Interfaces* **2009**, *1* (12), 2812–2820.

(21) (a) Monroe, C.; Newman, J. *J. Electrochem. Soc.* **2005**, *152*, A396–A404. (b) Monroe, C.; Newman, J. *J. Electrochem. Soc.* **2004**, *151*, A880–A886.

(22) Soo, P. P.; Huang, B.; Jang, Y.; Chiang, Y. M.; Sadoway, D. R.; Mayes, A. M. *J. Electrochem. Soc.* **1999**, *146* (1), 32–37.

(23) (a) Appetecchi, G. B.; Hassoun, J.; Scrosati, B.; Croce, F.; Cassel, F.; Salomon, M. *J. Power Source* **2003**, *124*, 246–253. (b) Saito, D.; Ito, Y.; Hanai, K.; Kobayashi, T.; Imanishi, N.; Hirano, A.; Takeda, Y.; Yamamoto, O. *J. Power Source* **2010**, *195*, 6172–6176. (c) Ueno, M.; Imanish, N.; Hanai, K.; Kobayashi, T.; Hirano, A.; Yamamoto, O.; Takeda, Y. *J. Power Source* **2011**, *196* (10), 4756–4761.

(24) Stephan, A. M.; Kumar, T. P.; Kulandainathan, M. A.; Lakshmi, N. A. *J. Phys. Chem. B* **2009**, *113* (7), 1963–1971.

(25) Croce, F.; Appetecchi, G. B.; Persi, L.; Scrosati, B. *Nature* **1998**, *394*, 456–458.

(26) (a) Liao, C. C.; Wu, H. Y.; Saikia, D.; Pan, Y. C.; Chen, Y. K.; Fey, G. T. K.; Kao, H. M. *Macromolecules* **2008**, *41*, 8956–8959. (b) Yu, X.; Xiao, M.; Wang, S.; Han, D.; Meng, Y. *J. Appl. Polym. Sci.* **2010**, *118*, 2078–2083. (c) Hassoun, J.; Panero, S.; Reale, P.; Scrosati, B. *Adv. Mater.* **2009**, *21*, 4807–4810. (d) Saikia, D.; Wu, H. Y.; Pan, Y. C.; Lin, C. P.; Huang, K. P.; Chen, K. N.; Fey, G. T. K.; Kao, H. M. *J. Power Source* **2011**, *196*, 2826–2834.

(27) Gowda, S. R.; Reddy, A. L. M.; Shaijumon, M. M.; Zhan, X.; Ci, L.; Ajayan, P. M. *Nano Lett.* **2011**, *11*, 101–106.

(28) Lee, H.; Cho, J. *Nano Lett.* **2007**, *7*, 2638–2641.

(29) (a) Yang, C.-S.; Bley, R. A.; Kauzlarich, S. M.; Lee, H. W. H.; Delgado, G. R. *J. Am. Chem. Soc.* **1999**, *121*, 5191–5195. (b) Warner, J. H.; Hoshino, A.; Yamamoto, K.; Tilley, R. D. *Angew. Chem., Int. Ed.* **2005**, *44*, 4550–4554.

(30) Hadjichristidis, N.; Iatrou, H.; Pispas, S.; Pitsikalis, M. *J. Polym. Sci., Part A: Polym. Chem.* **2000**, *38*, 3211–3234.

(31) (a) Wanakule, N. S.; Panday, A.; Mullin, S. A.; Gann, E.; Hexemer, A.; Balsara, N. P. *Macromolecules* **2009**, *42*, 5642. (b) Weber, R. L.; Ye, Y.; Schmitt, A. L.; Banik, S. M.; Elabd, Y. A.; Mahanthappa, M. K. *Macromolecules* **2011**, *44*, 5727–5735.

(32) Kim, S. Y.; Kim, S. H.; Park, M. J. *Nat. Commun.* **2010**, *1*, 88.

(33) Meyer, W. H. *Adv. Mater.* **1998**, *10* (6), 439–448.

(34) Sudeep, P. K.; Page, Z.; Emrick, T. *Chem. Commun.* **2008**, *46*, 6126–6127.

(35) Meyer, R.; Comtesse, D. *Phys. Rev. B* **2011**, *83*, 014301.

(36) Heimans, N. *Macromolecules* **2002**, *33*, 4226.

(37) Rubinstein, M.; Colby, R. H. In *Polymer Physics*; Oxford University Press Inc.: New York, 2003; p 53.

(38) Jacob, M. M. E.; Prabaharan, S. R. S.; Radhakrishna, S. *Solid State Ionics* **1997**, *104*, 267.

(39) Yang, Y.; Zhang, J.; Zhou, C.; Wu, S.; Xu, S.; Liu, W.; Han, H.; Chen, B.; Zhao, X. Z. *J. Phys. Chem. B* **2008**, *112*, 6594.

(40) (a) Brazier, A.; Dupont, L.; Dantras-Laffont, L.; Kuwata, N.; Kawamura, J.; Tarascon, J.-M. *Chem. Mater.* **2008**, *20* (6), 2352–2359. (b) White, H.; Pu, Y.; Rafailovich, M.; Sokolov, J.; King, A. H.; Giannuzzi, L. A.; Urbanik-Shannon, C.; Kempshall, B. W.; Eisenberg, A.; Schwarz, S. A.; Strzhemechny, Y. M. *Polymer* **2001**, *42*, 1613–1619.

(41) Pell, L. E.; Schricker, A. D.; Mikulec, F. V.; Korgel, B. A. *Langmuir* **2004**, *20*, 6546–6548.

(42) Aurbach, D.; Nimberger, A.; Markovsky, B.; Levi, E.; Sominski, E.; Gedanken, A. *Chem. Mater.* **2002**, *14*, 4155–4163.

(43) (a) Balaya, P.; Li, H.; Kienle, L.; Maier, J. *Adv. Funct. Mater.* **2003**, *13*, 621–625. (b) Ji, H.-X.; Wu, X.-L.; Fan, L.-Z.; Krien, C.; Fiering, I.; Guo, Y.-G.; Mei, Y.; Schmidt, O. G. *Adv. Mater.* **2010**, *22*, 4591–4595.

(44) (a) Kwon, Y.; Park, G. S.; Cho, J. *Electrochim. Acta* **2007**, *52*, 4663–4668. (b) Hu, Y.-S.; Demir-Caken, R.; Titrici, M. M.; Müller, J. O.; Schlögl, R.; Antonietti, M.; Maier, J. *Angew. Chem.* **2008**, *120*, 1669–1673. *Angew. Chem., Int. Ed.* **2008**, *47*, 1645.

(45) Chien, W.-M.; Chandra, D.; Lamb, J. H. *JCPDS-Int. Centre Diffr. Data* **2008**, *51*, 190.

(46) Hall., J. N.; Jones, J. W.; Sachdev, A. K. *Mater. Sci. Eng.* **1994**, *A183*, 69–80.

(47) Gordon, M. J.; Baron, T.; Dhalluin, F.; Gentile, P.; Ferret, P. *Nano Lett.* **2009**, *9* (2), 525.

(48) Nan, C. W.; Clarke, D. R. *Acta Mater.* **1996**, *44* (9), 3801.